International Journal of Coal Science & Technology (2023) 10:51
https://doi.org/10.1007/s40789-023-00613-5

RESEARCH

Pore structure of low-permeability coal and its deformation characteristics during the adsorption–desorption of CH_4/N_2

Pengfei Ji[1,3] · Haifei Lin[1,2,3] · Xiangguo Kong[1,2,3] · Shugang Li[1,2,3] · Biao Hu[1,3] · Pei Wang[1,3] · Di He[1,3] · Songrui Yang[1,3]

Received: 22 May 2023 / Revised: 20 July 2023 / Accepted: 28 July 2023

Abstract

The pore structure of coal plays a key role in controlling the storage and migration of CH_4/N_2. The pore structure of coal is an important indicator to measure the gas extraction capability and the gas displacement effect of N_2 injection. The deformation characteristic of coal during adsorption–desorption of CH_4/N_2 is an important factor affecting CH_4 pumpability and N_2 injectability. The pore structure characteristics of low-permeability coal were obtained by fluid intrusion method and photoelectric radiation technology. The multistage and connectivity of coal pores were analyzed. Subsequently, a simultaneous test experiment of CH_4/N_2 adsorption–desorption and coal deformation was carried out. The deformation characteristics of coal were clarified and a coal strain model was constructed. Finally, the applicability of low-permeability coal to N_2 injection for CH_4 displacement technology was investigated. The results show that the micropores and transition pores of coal samples are relatively developed. The pore morphology of coal is dominated by semi-open pores. The pore structure of coal is highly complex and heterogeneous. Transition pores, mesopores and macropores of coal have good connectivity, while micropores have poor connectivity. Under constant triaxial stress, the adsorption capacity of the coal for CH_4 is greater than that for N_2, and the deformation capacity of the coal for CH_4 adsorption is greater than that for N_2 adsorption. The axial strain, circumferential strain, and volumetric strain during the entire process of CH_4 and N_2 adsorption/desorption in the coal can be divided into three stages. Coal adsorption–desorption deformation has the characteristics of anisotropy and gas-difference. A strain model for the adsorption–desorption of CH_4/N_2 from coal was established by considering the expansion stress of adsorbed gas on the coal matrix, the compression stress of free gas on the coal matrix, and the expansion stress of free gas on micropore fractures. N_2 has good injectability in low-permeability coal seams and has the dual functions of improving coal seam permeability and enhancing gas flow, which can significantly improve the effectiveness of low-permeability coal seam gas control and promote the efficient utilization of gas resources.

Highlights

- The pore structure characteristics of low-permeability coal were obtained by fluid intrusion method and photoelectric radiation technology. The multistage and connectivity of coal pores were analyzed.
- A simultaneous test experiment of CH_4/N_2 adsorption–desorption and coal deformation was carried out. The deformation characteristics of coal were clarified and a coal strain model was constructed.
- The applicability of low-permeability coal to N_2 injection for CH_4 displacement technology was investigated.

✉ Pengfei Ji
17763563861@163.com

✉ Haifei Lin
lhaifei@xust.edu.cn

[1] College of Safety Science and Engineering, School of Safety Science and Engineering, Xi'an University of Science and Technology, 58, Yanta Mid. Rd., Xi'an 710054, Shaanxi, China

[2] Key Laboratory of Western Mine Exploitation and Hazard Prevention Ministry of Education, Xi'an University of Science and Technology, Xi'an 710054, Shaanxi, China

[3] Western Engineering Research Centre of Mine Gas Intelligent Drainage for Coal Industry, Xi'an 710054, Shaanxi, China

Published online: 15 September 2023

Keywords Low-permeability coal · Pore structure · Adsorption–desorption · Deformation characteristics · Strain model

1 Introduction

Coal is a complex porous medium, and its pore characteristics have an important impact on gas storage (adsorption) and migration (desorption–diffusion–seepage) (Zhang et al. 2022a). Coal pores can be divided into adsorption pores (< 100 nm) and seepage pores (> 100 nm). The former is the main space for gas adsorption, desorption, and diffusion, and the latter is the main channel for gas seepage (Sang et al. 2005; Lu 2016). The fine characterization of coal pore structure is of great significance for the in-depth study of gas adsorption and desorption characteristics and coal deformation characteristics (Wen et al. 2023; Wang et al. 2022). Low-temperature gas adsorption, high-pressure mercury intrusion, and low-field nuclear magnetic resonance (NMR) are commonly used in the coal industry to determine the pore structure of coal, resulting in a variety of coal pore division types (Hu et al. 2023; Cheng and Hu 2023; Hodot 1966). Among them, the HODOT B.B. pore classification method is widely accepted because it fully considers the flow characteristics of gases in pore structures of different sizes: micropores (< 10 nm), transition pores (10–100 nm), mesopores (100–1000 nm), and macropores (1–100 μm).

Both coal mining and gas extraction involve issues such as the interaction between coal and gas, and the mechanical behavior of gas adsorption–desorption (Zhu et al. 2018; Lin et al. 2023a). In-depth research on gas adsorption–desorption characteristics and coal deformation characteristics is of great significance to improve the effectiveness of gas extraction. In the past, researchers mostly started from the adsorption expansion and desorption shrinkage deformation characteristics of coal, and introduced the coal deformation coefficient to establish models to characterize the relationship between coal adsorption deformation and gas adsorption amount or desorption deformation and gas desorption amount (Zhang et al. 2022b, 2021). And the Langmuir-like equation is often used to describe the coal deformation characteristics of adsorption expansion/desorption shrinkage (Lin et al. 2017). Related studies have shown anisotropy in coal deformation during gas adsorption/desorption. The mechanical strength of coal also decreases after gas adsorption, and the elastic modulus will decrease at the macroscopic level, which is inconsistent with the assumptions of conventional models describing coal deformation (He et al. 2018; Ranjith et al. 2010). The applicability and reliability of the existing coal deformation models need to be further investigated.

Based on the pore structure parameters of low-permeability coal measured by low-temperature gas adsorption, high-pressure mercury intrusion, and low-field NMR experiments, the author conducted a detailed characterization of the coal pore structure and obtained the fractal characteristics and tortuous connectivity of the coal pore structure. The simultaneous test experiments of CH_4/N_2 adsorption–desorption and coal deformation were carried out by using the flow-solid coupling experimental system for coal seam gas. The influence law of gas type/gas pressure on coal deformation is quantitatively characterized. A strain model for coal at each stage of CH_4/N_2 adsorption–desorption was constructed. The applicability of coal samples to the N_2 injection for CH_4 displacement technology is investigated. To provide a theoretical basis for high-efficiency extraction of gas from low-permeability coal seams.

2 Experimental schemes

2.1 Experimental coal samples

2.1.1 Parameters determination and preparation of coal samples

Coal samples were collected from low-permeability mines in the Qinshui Basin, China. The basic parameters were determined after sampling, as shown in Table 1. Coal pore structure characterization experiments take pulverized coal, granular coal, and cylindrical standard coal samples as research objects. The coal samples are taken from large coal blocks without gangue, and the specific sample specifications are prepared according to the equipment requirements. The simultaneous test experiment of CH_4/N_2 adsorption–desorption and coal deformation takes the cylindrical standard coal samples as the research object. Pulverized coal, granular coal, and Φ50 mm × 100 mm cylindrical standard coal samples are shown in Fig. 1a.

Table 1 Basic parameters of the coal samples

Industrial analysis				Compressive strength (MPa)	Elastic modulus (10^3 MPa)	Poisson's ratio
Moisture (%)	Ash (%)	Volatile (%)	Fixed carbon (%)			
2.08	7.19	30.00	61.50	25.10	3.50	0.31

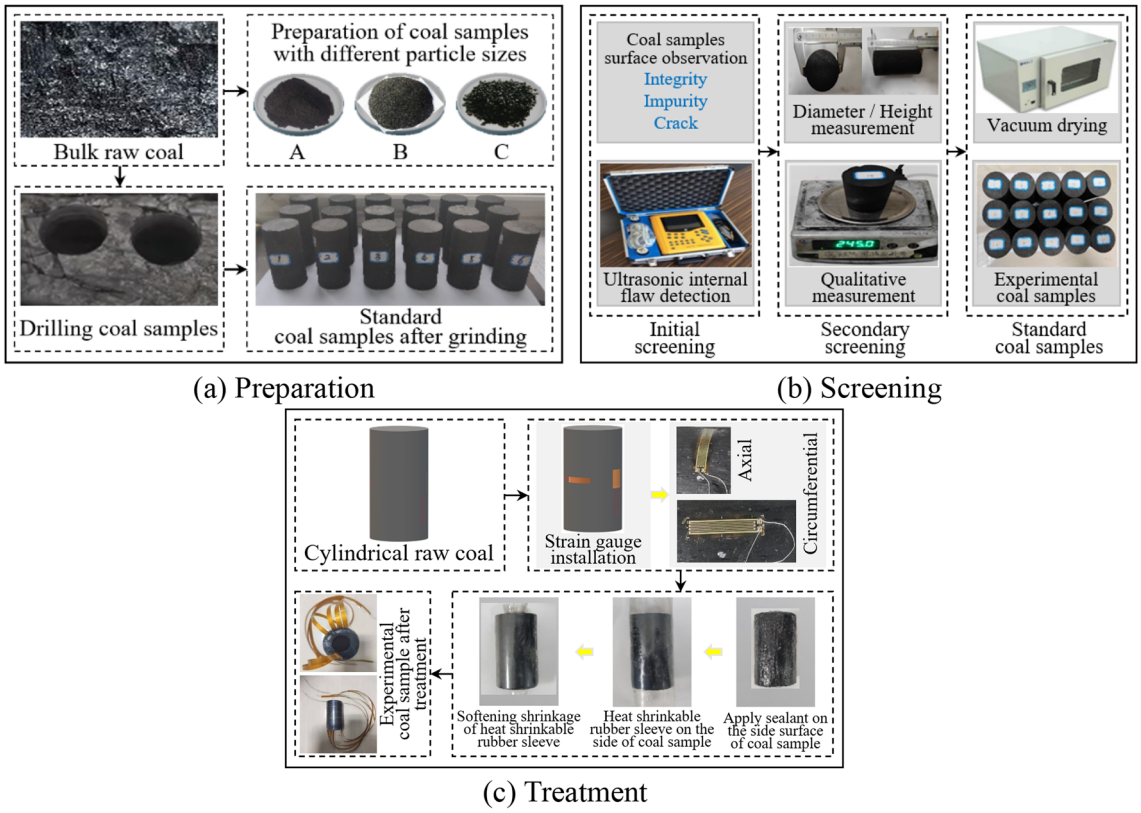

Fig. 1 Experimental coal samples

2.1.2 Screening and treatment of coal samples

The screening process of the cylindrical standard coal samples consists of initial screening and secondary screening, as illustrated in Fig. 1b. (1) Initial screening: Select coal samples with neat ends, no impurities, and no cracks. Subsequently, the non-metallic acoustic detector is used to detect the internal defects of the coal and screen out the coal samples with uniform texture. (2) Secondary screening: The height, diameter, and quality of the coal samples were measured, and those with excessively different values were rejected. Subsequently, the screened coal samples are dried to constant weight by using a vacuum drying oven.

The handling process of cylindrical standard coal samples includes strain gauge installation and sealing treatment, as depicted in Fig. 1c. (1) Strain gauge installation: Two strain gauges are installed on the side surface along the axial/radial direction of the coal sample to monitor the deformation of the coal sample in real-time. (2) Sealing treatment: Apply sealant to the side surface of the coal sample and let it air-dry. Then, a heat-shrinkable rubber sleeve is applied and a blower is used to soften and shrink the heat-shrinkable rubber sleeve. Finally, sealant is applied to the edges of both ends of the coal sample and let it air-dry to prevent gas from escaping during the experiment.

2.2 Characterization experiment of coal pore structure

Coal pore structure characterization experiments include: (1) Low-pressure CO_2 adsorption experiment, low-temperature N_2 adsorption experiment: Determination of micropore and transition pore parameters of coal samples, and the sample specifications are 60–80 mesh coal powder. (2) High-pressure mercury intrusion experiments: To determine the mesopore and macropore parameters of coal samples, and the sample specifications are 3.0–4.0 mm coal particles. (3) Low-field NMR experiment: To determine the pore parameters of cylindrical standard coal samples.

2.3 Experiment on the deformation characteristics of coal

2.3.1 Experimental system

The simultaneous experiment of CH_4/N_2 adsorption–desorption and coal deformation was carried out by the flow-solid coupling experimental system for coal seam gas of Xi'an University of Science and Technology. The system mainly consists of a stress loading system, axial/circumferential strain measurement and acquisition system, gas data

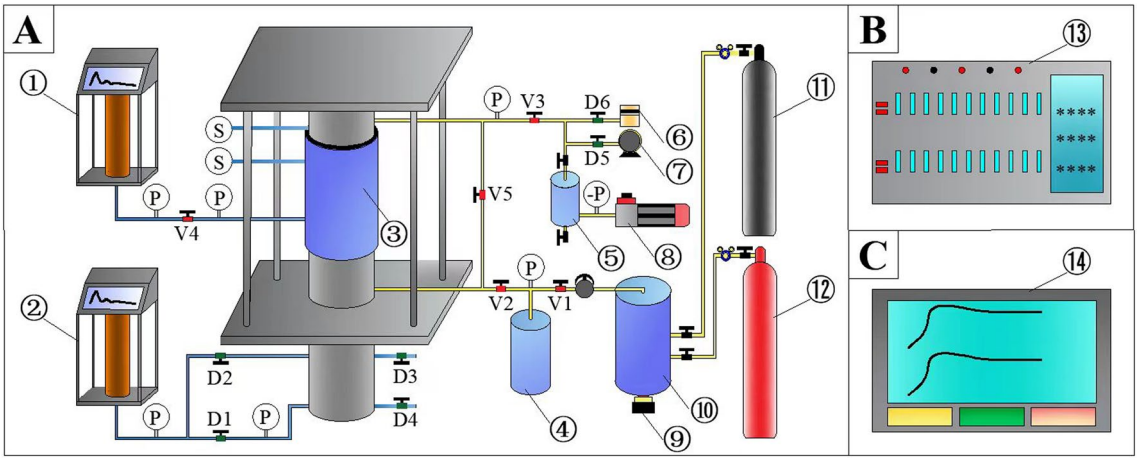

Fig. 2 Experimental system (Lin et al. 2023b). A-1 Confining pressure loading pump, A-2 Axial pressure loading pump, A-3 Temperature control system, A-4 Gas buffer tank, A-5 Vacuum buffer tank, A-6 Precision flowmeter, A-7 Wet flowmeter, A-8 Vacuum pump, A-9 Mixed pump, A-10 Mixing tank, A-11 High-pressure N_2 cylinder, A-12 High-pressure CH_4 cylinder, A-S Displacement sensor, A-P Pressure sensor, A-V1–A-V5 Manual valve, A-D1–A-D6 Electromagnetic valve, B-13 Axial/Circumferential strain measurement system, C-14 Gas data measurement system

measurement and acquisition system (collect gas pressure data in real-time, and calculate gas adsorption and desorption volumes under different equilibrium pressures based on coal sample quality and gas pressure.), temperature control system, evacuation system, and auxiliary system, as described in Fig. 2.

2.3.2 Experimental condition and process

In order to investigate the CH_4/N_2 adsorption–desorption law and the deformation characteristics of coal during the whole experiment, the experimental conditions were designed by the controlled variable method. The initial gas adsorption pressure, the experimental temperature, and the axial pressure/confining pressure loaded on the coal (according to the buried depth of the coal seam, the bulk density of the overlying strata, and the gas pressure, as well as combined with the similarity theory to calculate) are set according to the gas occurrence characteristics of the coal seam at the sampling location. According to the field measurement and theoretical calculation, the axial pressure/confining pressure was set to 2.5/2.0 MPa, the experimental temperature was set to 303 K, and the initial CH_4/N_2 adsorption pressure was set to five pressure gradients (0.74 MPa, 0.94 MPa, 1.14 MPa, 1.34 MPa, and 1.54 MPa).

Experimental steps: (1) Coal sample installation. Apply axial pressure/confining pressure to the preset pressure step by step on the sealed coal sample. (2) Airtightness test. Fill the reactor with a certain pressure of He and leave it for 6 h. The air pressure value remains unchanged to prove good airtightness. (3) Free space volume calibration. Calibrate the total free volume, the free volume at the inlet end, and the free volume at the exhaust end of the experimental system. (4) Vacuum degassing. The coal samples were degassed under vacuum for 6 h. (5) Gas adsorption equilibrium. Adsorb gas at a preset gas pressure. The coal strain of the process is collected, and when the air-pressure value and the strain curve are stable at the same time, it indicates that the adsorption has reached equilibrium. (6) Gas desorption equilibrium. The coal samples with adsorption equilibrium were desorbed under atmospheric pressure. The coal strain of the process is collected and when the flow meter indicates 0, it is determined that the desorption has reached equilibrium.

3 Joint characterization of pore structure in low-permeability coal

3.1 Multimethod for determination of coal pore structure

The micropore distribution characteristics of coal samples were obtained by the low-pressure CO_2 adsorption experiment, as presented in Fig. 3a. The pore diameter of coal samples has peaks at 0.35 nm, 0.48 nm, 0.55 nm, and 0.83 nm. Among them, the half-peak width at 0.35 nm is narrower, the half-peak width at 0.83 nm is wider, and the pores at 0.48 nm and 0.55 nm have the largest distribution. The distribution characteristics of transition pores/mesopores in coal samples were obtained by the low-temperature N_2 adsorption experiment, as illustrated in Fig. 3b. The pore-size distribution of the coal samples was bimodal, with the

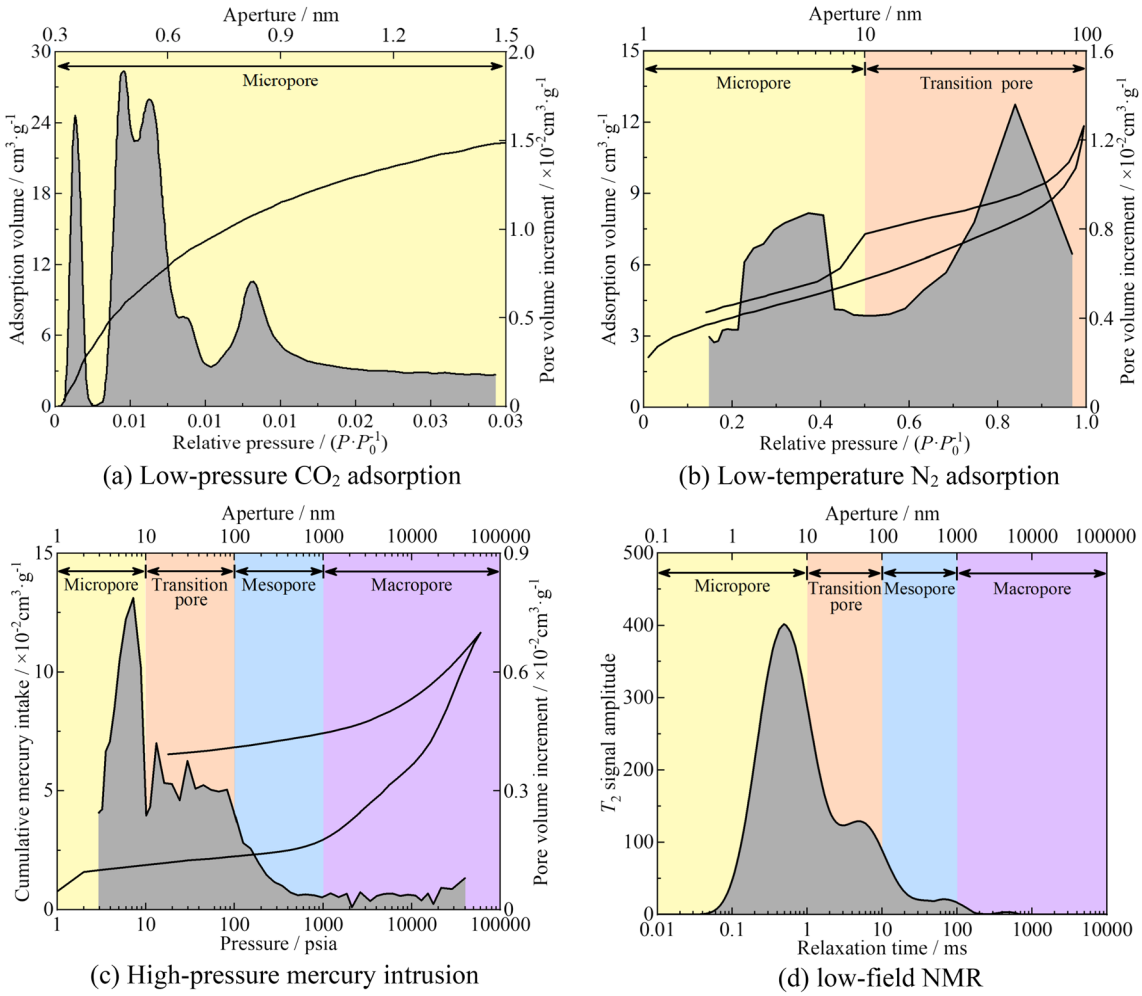

Fig. 3 Multimethod for determination of coal pore structure

peak at 50 nm higher than the peak at 5 nm. There is a significant adsorption hysteresis phenomenon in the adsorption curve, which is related to the capillary coalescence phenomenon that occurs in the high relative pressure region (Li et al. 2023). According to the IUPAC classification of hysteresis loop, the coal sample is consistent with the H2 type hysteresis loop, indicating that the coal contains a high number of semi-open pores (wedge type, ink bottle type), which are conducive to gas adsorption and storage, but not conducive to gas migration (Gregg and Sing 1982).

The distribution characteristics of mesopores/macropores of coal samples were obtained by the high-pressure mercury intrusion experiment, as depicted in Fig. 3c. There is an obvious mercury intrusion hysteresis loop in the mercury intrusion curve, indicating that the pores of the coal samples are mostly semi-closed pores with poor pore connectivity, which is corroborated by the results of the low-temperature N_2 adsorption experiment. The results of the low-field NMR experiment are shown in Fig. 3d. The T_2 distribution curve was in the shape of three peaks. The relaxation times of the wave peaks were distributed at 0.5 ms, 5.0 ms, and 70.0 ms, and mainly concentrated at 0.5 ms, indicating that the micropores and transition pores of the coal samples were relatively developed.

3.2 Multimethod for joint characterization of coal pore structure

Low-pressure CO_2 adsorption, low-temperature N_2 adsorption, and high-pressure mercury intrusion all have their dominant pore-size segments (pore-size ranges with high test accuracy). To finely characterize the coal pore structure, the dominant pore-size segments of each test method were stitched together. Related studies have shown that low-pressure CO_2 adsorption is an ideal tool for micropore testing, which can accurately characterize the micropore distribution at < 2 nm (Liu et al. 2021). Low-temperature N_2 adsorption has high testing accuracy for micropores/transition pores

(2–50 nm) (Lin et al. 2019). High-pressure mercury intrusion can be tested for mesopores/macropores. Due to the compressibility of coal, when the mercury injection pressure is > 10 MPa, the coal matrix is prone to compressive deformation/destruction, which will affect the accuracy of the experiment. Therefore, high-pressure mercury intrusion was chosen to characterize the pore distribution at > 50 nm (Liu et al. 2022).

The joint characterization results of the coal pore-size (Fig. 4) show that the pore-size distribution of the coal samples is multi-peaked and dominated by micropores (which provide a high number of adsorption vacancies for gas adsorption), with a certain proportion of transition pores and mesopores, and the smallest proportion of macropores.

Fractal theory is widely used to characterize the complexity of coal pore structure. There are various methods to calculate the fractal dimension and each has its own characteristics (Jiang et al. 2021). The FHH model is suitable for characterizing the fractal features of the pore structure in micropores and transition pores (Jia et al. 2021). The Menger model is suitable for characterizing the fractal features of the pore structure in mesopores/macropores (Chen et al. 2020). The fractal characteristics of the pore structure in coal samples are shown in Table 2.

From the low-temperature N_2 adsorption curve, it can be known that the gas adsorption mechanism is different for $P/P_0 > 0.5$ and $P/P_0 < 0.5$. For this purpose, the fractal dimension of both (D_{11}, D_{12}) was calculated separately using the FHH model. The fractal dimension of the pore structure for pore-size < 100 nm is obtained. It is calculated that $D_{11} = 2.85 < D_{12} = 2.54$, which indicates that the pore structure of the micropores and transition pores in coal samples is generally complex, and the pore structure of micropores is more complex. According to the experimental data of high-pressure mercury intrusion, the Menger model was used to calculate the fractal dimension of the pore structure with pore-size > 100 nm. It is calculated that $D_2 = 2.61 < 3$, which indicates that the pore structure of mesopores and macropores in coal samples is equally complex. Altogether, the pore structure complexity of micropores in coal samples was greater than that of mesopores/macropores than that of transition pores.

3.3 Tortuous connectivity of coal pore structure

Tortuosity (τ) is a pore characterization parameter that quantitatively characterizes the tortuosity of the seepage channel. Tortuosity is defined as the ratio of the actual length of the seepage channel to the apparent length through the seepage medium (Dullien 2012; Attia 2005; Yu et al. 2003). It is calculated that $\tau = 5.81$, which indicates that the seepage channel of the coal sample is tortuous and the gas flow is difficult. In low-permeability coal, the pores are mostly closed-pores, so the degree of pore connectivity also needs to be considered. The total porosity, effective porosity, and residual porosity of the

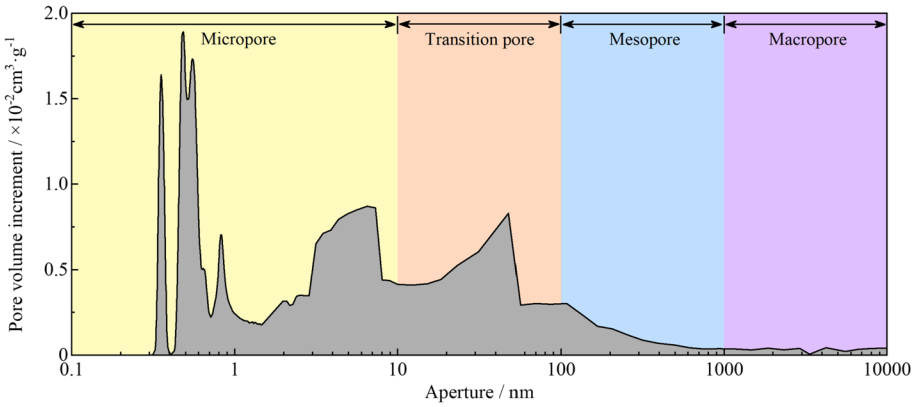

Fig. 4 Fine characterization of coal pore structure

Table 2 Fractal dimension of pore structure based on FHH model/Menger model

Aperture	Model	Fitting equation	Fractal dimension	R^2
Micropore	FHH	$\mathrm{Ln}V = 1.74 - 0.15\ln[\ln(P_0/P)]$	$D_{11} = 2.85$	0.95
Transition pore	FHH	$\mathrm{Ln}V = 1.55 - 0.46\ln[\ln(P_0/P)]$	$D_{12} = 2.54$	0.99
Mesopore/Macropore	Menger	$\lg[\mathrm{d}V/\mathrm{d}P] = -2.72 - 1.39\lg P$	$D_2 = 2.61$	0.97

Note: V is the pore volume corresponding to the relative pressure, cm^3/g; P_0 is the saturated vapor pressure of the adsorbed gas; MPa; P is the system equilibrium pressure, MPa

coal samples were calculated based on the T_2 distribution curves in the saturation/centrifugation condition, and then the pore connectivity rate was obtained, as described in Fig. 5a, b. The effective porosity of the coal sample was calculated to be 3.04%, and the pore connectivity rate was 40.36%. The pore connectivity rate of pore-size < 10 nm is relatively low, indicating that the pore connectivity of transition pores, mesopores and macropores in coal samples is good, and the pore connectivity of micropores is poor.

It can be known that the pore connectivity is related to the pore-size. The relationship between pore connectivity rate, pore percentage, and pore-size is shown in Fig. 5c. As the pore-size increases, the proportion of pores in each pore-size segment decreases, while the pore connectivity rate shows a gradual trend. The pore connectivity rates of < 10 nm, 10–100 nm, 100–1000 nm, and > 1000 nm pore-size segments were 10.96%, 91.36%, 96.32%, and 100%, respectively. It is due to the pore-size of micropores is small, which has a lower probability of forming connected pore groups, resulting in a weak pore connectivity rate. However, the pore-size of transition pores, mesopores and macropores is larger, which has a higher probability of forming connected pore groups, resulting in a higher pore connectivity rate.

4 Experimental results of coal deformation characteristics

4.1 Adsorption and desorption characteristics of CH_4/N_2

The variation pattern of CH_4/N_2 adsorption amount with experimental time is shown in Fig. 6. With the prolongation of the adsorption time, the adsorption amount of CH_4/N_2 showed a trend of rapid growth—slow growth—flattening. As the gas pressure increases, the adsorption amount of CH_4/N_2 gradually increases. When the gas pressure increased from 0.74 to 1.54 MPa, the adsorption amount of CH_4 and N_2 increased by 111.11% and 76.92%, respectively. With the prolongation of the desorption time, the adsorption amount of CH_4/N_2 presents a trend of rapid decrease—slow decrease—leveling. As the gas pressure increases, the amount of CH_4/N_2 desorption gradually increases. When the gas pressure increased from 0.74 to 1.54 MPa, the desorption amount of CH_4 and N_2 increased by 132.07% and 90.87%, respectively.

Existing studies have shown that the variation law of CH_4/N_2 adsorption amount with adsorption time and desorption time conforms to the Langmuir-type equation (Eq. (1)) (Meng et al. 2021). Fitting the experimental data of the adsorption amount of CH_4 and N_2 are found (Table 3): The value of A_a increases with the increase of gas pressure, and the value of B_a shows an overall increasing trend, indicating that increasing the gas pressure not only increases the amount of CH_4/N_2 adsorbed by coal, but also effectively increases the adsorption energy (adsorption interaction between coal molecules and gas molecules), resulting in a sharp increase in the adsorption amount curve. The A_d value increases with the increase of gas pressure, and the overall change of B_d value is not significant, indicating that increasing the gas pressure has the same promoting effect on enhancing the amount of CH_4/N_2 desorbed from the coal.

$$\begin{cases} Q_a = A_a B_a t_a / (1 + B_a t_a) \\ Q_d = C_d - A_d B_d t_d / (1 + B_d t_d) \end{cases} \quad (1)$$

where, Q_a is the gas adsorption amount at the time of t_a, mol; A_a is the gas saturation adsorption amount, mol; B_a is the constant related to the adsorption time, s^{-1}; t_a is the adsorption time, s; Q_d is the gas adsorption amount at the time of t_d, mol; C_d is the gas adsorption amount at the adsorption equilibrium, mol; A_d is the ultimate gas desorption amount, mol; B_d is the constant related to the desorption time, s^{-1}; t_d is the desorption time, s.

The CH_4/N_2 adsorption amount-desorption amount-residual adsorption amount after coal adsorption/desorption equilibrium is shown in Table 4. As the gas pressure increases, the amount of CH_4 and N_2 adsorbed/desorbed by the coal increases. Under the same gas pressure, the amount of CH_4 adsorbed by the coal is greater than that of N_2, the amount of CH_4 desorbed by the coal is greater than that of N_2, and the amount of residual CH_4 adsorbed by the coal is greater than that of N_2. Under different gas pressures, the residual adsorption volumes of CH_4 and N_2 were 55.2–79.0 and 13.2–28.2 mL, respectively.

4.2 Deformation characteristics of coal

The variation pattern of the adsorption strain/desorption strain of coal with experimental time is shown in Fig. 7. In the adsorption process, the axial strain/volumetric strain of coal can be divided into three stages: initial compressive strain, adsorption expansion strain, and strain equilibrium. The circumferential strain is divided into three stages: initial expansion strain, adsorption expansion strain, and strain equilibrium (Lin et al. 2023b). For the desorption process, the axial strain/volumetric strain of coal is divided into three stages: initial expansion strain, desorption shrinkage strain, and strain equilibrium. The circumferential strain is divided into three stages: initial compression strain, desorption shrinkage strain, and strain equilibrium.

The main reasons are: (1) Initial expansion/compression strain stage: After the gas desorption experiment starts,

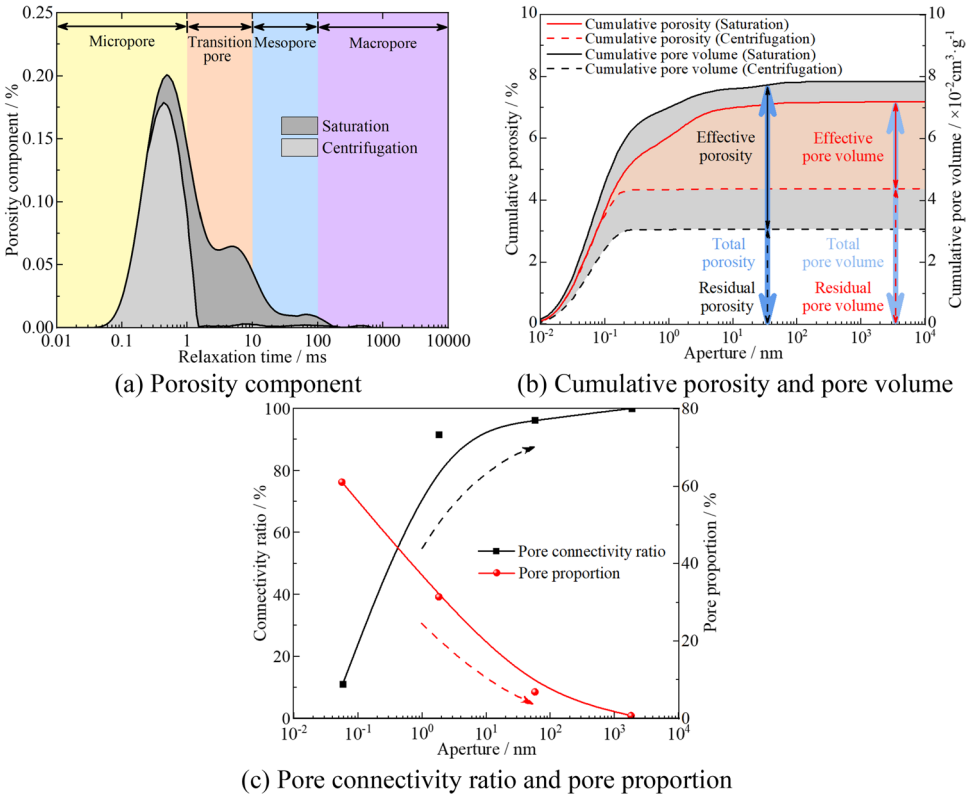

(a) Porosity component

(b) Cumulative porosity and pore volume

(c) Pore connectivity ratio and pore proportion

Fig. 5 Tortuous connectivity of coal pore structure

the gas pressure at the exhaust end is instantly deflated, the force in the axial direction of coal is reduced, and the expansion deformation occurs first in the axial direction and the shrinkage deformation occurs first in the circumferential direction. (2) Desorption shrinkage strain stage: Coal continuously desorbs gas and its shrinkage deformation occurs. (3) Strain equilibrium stage: With the extension of the desorption time, the gas no longer precipitates out of the coal, and the axial/circumferential strain of the coal tends to be smooth.

Existing studies show that the variation law of coal strain with adsorption time/desorption time follows the Langmuir-type equation (Eq. (2)) (Li et al. 2018). Fitting the experimental data of coal strain revealed (Table 5):

$$\begin{cases} \varepsilon_a = D_a E_a t_a/(1+E_a t_a) + F_a \\ \varepsilon_d = F_d + G_d - D_d E_d t_d/(1+E_d t_d) \end{cases} \quad (2)$$

where, ε_a is the strain generated by the adsorbed gas of coal at the time of t_a, με; D_a is the ultimate expansion strain generated by the adsorbed gas of coal, με; E_a is the constant associated with the adsorption time, s^{-1}; F_a is the initial compression/expansion strain of coal during the adsorption process, με; ε_d is the strain generated by the adsorbed gas of coal at the time of t_d, με; F_d is the equilibrium strain of the adsorbed coal, με; G_d is the initial compression/expansion strain of the desorbed coal during desorption, με; D_d is the ultimate shrinkage strain generated by the desorbed gas of coal, με; E_d is the constant related to the desorption time, s^{-1}.

(1) When coal adsorbs CH_4, D_a and E_a increase with the increase of gas pressure. When coal adsorbs N_2, D_a increases with the increase of gas pressure and E_a shows an overall increasing trend. Under the same gas pressure, D_a for CH_4 adsorption is greater than D_a for N_2 adsorption. E_a for CH_4 adsorption is less than E_a for N_2 adsorption. The above phenomenon shows that increasing the gas pressure not only improves the adsorption expansion amount of coal, but also effectively enhances the expansion strain energy (the difficulty of coal expansion caused by gas adsorption), resulting in a sharp increase in the strain curve. Under the same gas pressure, the adsorption expansion ability of coal when adsorbing CH_4 is stronger than that of N_2, but the expansion strain energy when adsorbing CH_4 is weaker than that of N_2 (Jin and Huang 2015).

(2) When coal desorbs CH_4/N_2, D_d increases with the increase of gas pressure and E_d shows an overall increasing trend. At the same gas pressure, D_d for the

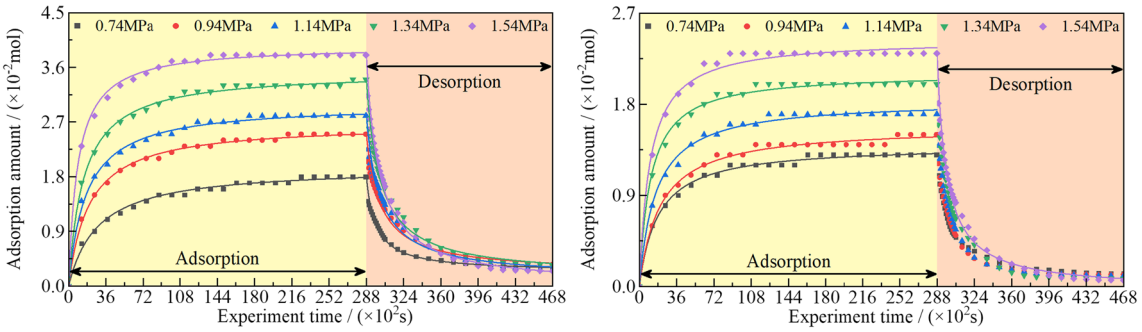

Fig. 6 Adsorption amount of CH_4/N_2

Table 3 Fitting parameters of CH_4/N_2 adsorption amount

Gas type	Stage	Fitting parameter	Gas pressure (MPa)					Stage	Fitting parameter	Gas pressure (MPa)				
			0.74	0.94	1.14	1.34	1.54			0.74	0.94	1.14	1.34	1.54
CH_4	I	$A_a(\times 10^{-2})$	1.96	2.68	3.00	3.53	3.96	II	$A_d(\times 10^{-2})$	1.57	2.28	2.67	3.25	3.81
		$B_a(\times 10^{-4})$	3.53	5.00	5.91	6.85	11.30		$B_d(\times 10^{-4})$	11.00	7.46	7.39	7.72	8.12
		R^2	0.99	0.99	0.99	0.99	0.99		R^2	0.98	0.98	0.97	0.98	0.99
N_2	I	$A_a(\times 10^{-2})$	1.40	1.58	1.84	2.11	2.44	II	$A_d(\times 10^{-2})$	1.23	1.47	1.70	2.05	2.33
		$B_a(\times 10^{-4})$	5.53	5.00	6.32	9.24	9.73		$B_d(\times 10^{-4})$	10.90	12.20	11.60	10.60	11.10
		R^2	0.98	0.98	0.98	0.96	0.98		R^2	0.99	0.99	0.99	0.99	0.98

Note: I represents the adsorption process. II represents the desorption process

desorption of CH_4 from coal is greater than D_d for the desorption of N_2. E_d for the desorption of CH_4 from coal is less than E_d for the desorption of N_2. The above phenomenon shows that increasing the gas pressure not only improves the desorption shrinkage amount of coal but also effectively enhances the shrinkage strain energy (the difficulty of coal shrinkage deformation caused by gas desorption), resulting in a sharp decrease in the strain curve. Under the same gas pressure, the shrinkage deformation ability of coal when desorbing CH_4 is stronger than that of N_2, but the shrinkage strain energy when desorbing CH_4 is weaker than that of N_2.

The residual adsorption strain of coal after desorption of CH_4/N_2 equilibrium at different gas pressures is shown in Fig. 8. The total residual adsorption strain of coal shows that the volume residual adsorption strain is greater than the axial residual adsorption strain than the circumferential residual adsorption strain. The residual adsorption strain generated when coal adsorbs CH_4 is greater than that generated when coal adsorbs N_2. This is because the residual adsorption amount of CH_4 in coal is greater than the residual adsorption amount of N_2 after the gas desorption reaches the equilibrium state.

With the increase of CH_4 pressure, the decreased rate of residual adsorption strain of coal gradually increases. While with the increase of N_2 pressure, the decreased rate of residual adsorption strain of coal remains unchanged. The reason is that coal has a very strong adsorption capacity for CH_4 (under the same equilibrium pressure condition, the reduction of surface free energy when coal adsorbs CH_4 is greater than that of adsorbing N_2). According to the theory proposed by Bangham that the amount of solid expansion deformation is proportional to the amount of surface free energy reduction (Xie and Huang 1985), it can be known that the more gas adsorbed by coal, the greater the reduction in surface free energy, the greater the expansion deformation caused by gas adsorption, and the more obvious the weakening damage to the coal. Therefore, the modification effect of adsorbed CH_4 on the pore structure of coal is stronger than that of adsorbed N_2. And the higher the pressure of CH_4, the more significant the modification effect on the pore structure, resulting in an increase in the reduction rate of the residual adsorption strain in the coal.

Table 4 Adsorption amount, desorption amount and residual adsorption amount

Gas type	Gas volume (mol)	Gas pressure (MPa)					Gas type	Gas volume (mol)	Gas pressure (MPa)				
		0.74	0.94	1.14	1.34	1.54			0.74	0.94	1.14	1.34	1.54
CH_4	Adsorption amount/$\times 10^{-2}$	1.80	2.50	2.80	3.40	3.80	N_2	Adsorption amount/$\times 10^{-2}$	1.30	1.50	1.70	2.00	2.30
	Desorption amount/$\times 10^{-2}$	1.53	2.15	2.54	3.06	3.55		Desorption amount/$\times 10^{-2}$	1.17	1.38	1.59	1.92	2.24
	Residual adsorptionamount/$\times 10^{-3}$	2.69	3.53	2.60	3.42	2.46		Residual adsorptionamount/$\times 10^{-3}$	1.26	1.16	1.06	0.76	0.59

4.3 Correlation between coal deformation and gas adsorption amount

The relationship between the adsorption expansion strain of coal and the equilibrium adsorption amount of CH_4/N_2 is shown in Figs. 9a, b. The expansion strain of coal adsorbed CH_4 is greater than that of adsorbed N_2 for the same amount of adsorption. The expansion strain of the coal increases exponentially as a function of CH_4 adsorption. The adsorption expansion strain rate gradually decreases with the increase of CH_4 adsorption, and the axial strain rate changes significantly. The adsorption expansion strain of coal shows a one-dimensional growth function with the increase of N_2 adsorption amount (ε_1, ε_2, and ε_3 are the axial strain, circumferential strain, and volumetric strain of the coal during the adsorption process, q_1 is the CH_4/N_2 adsorption amount, $H_{ac} - I_{an}$ is related fitting constants).

The main reason is that the bedding of the experimental coal sample is perpendicular to the axial direction of the coal. When the coal adsorbs gas, the bedding has strong adsorption deformation amount, and the coal has stronger adsorption amount for CH_4 than for N_2. As the amount of CH_4 adsorption increases, the adsorption vacancies in the coal are continuously occupied by CH_4 molecules, resulting in a large expansion strain, and this strain first appears in the direction vertical to the bedding plane, resulting in a larger axial strain rate of the coal when the adsorption amount is small. As the adsorption continues, the remaining adsorption vacancies in the coal decrease, and the expansion strain rate caused by adsorption decreases, which shows that the axial strain rate of the coal decreases with the increase of the adsorption amount when adsorbing CH_4.

The relationship between coal desorption shrinkage strain and CH_4/N_2 equilibrium desorption amount is shown in Figs. 9c, d. Under the same amount of desorption, the shrinkage strain of coal desorbed CH_4 is greater than that of desorbed N_2. The desorption shrinkage strain of coal increases exponentially as a function of CH_4 desorption, and the desorption shrinkage strain rate decreases gradually with the increase of N_2 desorption amount, and the change of axial strain rate is obvious. The desorption shrinkage strain of coal increases with the increase of N2 desorption amount as a linear function of one variable (ε_4, ε_5, ε_6 are the axial strain, circumferential strain, and volumetric strain of the coal during the desorption process, q_2 is the desorption amount of CH_4/N_2, $H_{dc} - I_{dn}$ are related fitting constants) (Table 6).

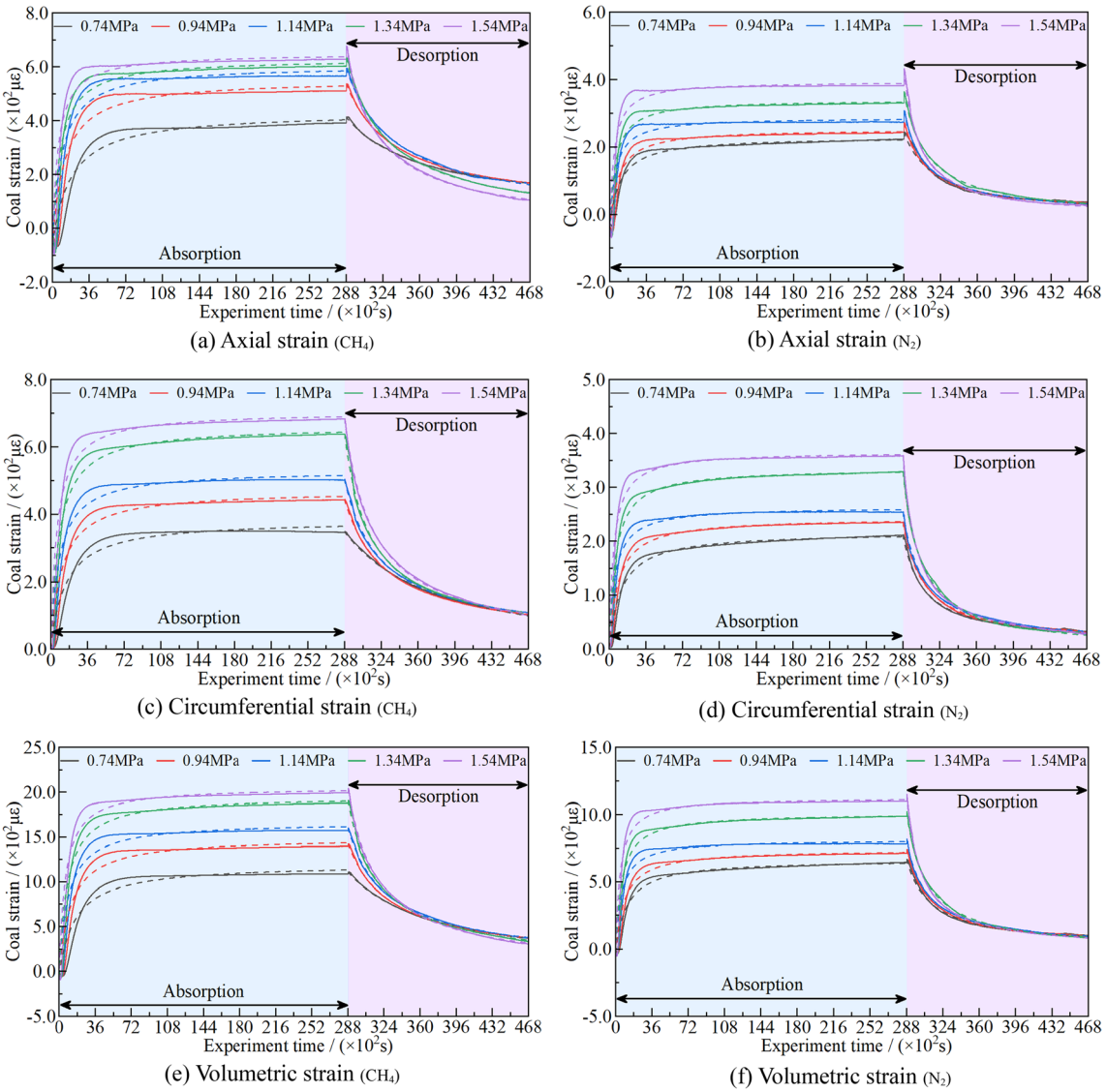

Fig. 7 Axial strain/circumferential strain/volumetric strain characteristics of coal

5 Discussion

5.1 Gas occurrence pattern and coal deformation characteristics in complex pore

5.1.1 Gas occurrence pattern

The form of gas occurrence in coal is the basis for the investigation of its adsorption–desorption–diffusion–seepage characteristics. There are differences in the forms of gas occurrence within pores with different sizes. Among them, the adsorption force fields of the micropores superimpose the potential energy, resulting in gas enrichment mainly in the form of filling. Larger pores are dominated by gas surface coverage (Cheng and HU B. 2021). Related studies have shown that the van der Waals force on gas molecules is significantly enhanced in < 1.5 nm micropores, while the forces generated between gas molecules and pore-walls in larger pores have a relatively limited range of influence. This is because the gas adsorption in the > 1.5 nm pore-size segment belongs to supercritical adsorption and is dominated by monomolecular layer adsorption (Ortiz et al. 2016). Based on the difference of van der Waals forces on gas molecules in pores with different sizes, < 1.5 nm micropores can be divided into the strong-adsorption potential region (forced by the micropore wall) and the weak-adsorption potential region (force between adjacent gas molecules). Transition pores, mesopores, and macropores can be divided into

Table 5 Fitting parameters of axial/circumferential/volumetric strain of coal

Gas type	Stage	Strain	Fitting parameter	Gas pressure (MPa)					Stage	Strain	Fitting parameter	Gas pressure (MPa)				
				0.74	0.94	1.14	1.34	1.54				0.74	0.94	1.14	1.34	1.54
CH_4	I	i	$D_a(\times 10^2)$	4.99	6.22	6.84	7.20	7.46	II	i	$D_d/\times 10^2$	3.51	4.72	5.49	6.18	6.70
			$E_a(\times 10^{-4})$	5.67	8.67	11.30	13.80	19.30			$E_d/\times 10^{-4}$	1.30	1.99	2.07	2.39	3.17
			R^2	0.90	0.88	0.89	0.90	0.90			R^2	0.99	0.99	0.99	0.99	0.99
		ii	$D_a(\times 10^2)$	3.79	4.67	5.27	6.60	7.02		ii	$D_d/\times 10^2$	3.81	4.19	4.72	6.05	6.70
			$E_a(\times 10^{-4})$	6.79	9.10	11.80	12.20	16.10			$E_d/\times 10^{-4}$	1.04	2.40	2.82	3.95	3.49
			R^2	0.91	0.92	0.92	0.94	0.93			R^2	0.99	0.99	0.99	0.99	0.99
		iii	$D_a(\times 10^3)$	1.25	1.55	1.73	2.02	2.15		iii	$D_d/\times 10^3$	1.11	1.31	1.49	1.81	2.00
			$E_a(\times 10^{-4})$	6.21	8.86	11.50	12.60	17.20			$E_d/\times 10^{-4}$	1.10	2.24	2.51	3.34	3.34
			R^2	0.91	0.91	0.91	0.93	0.92			R^2	0.99	0.99	0.99	0.99	0.99
N_2	I	i	$D_a(\times 10^2)$	2.66	3.05	3.47	4.06	4.63	II	i	$D_d/\times 10^2$	2.50	2.71	3.08	3.75	4.44
			$E_a(\times 10^{-4})$	9.60	12.80	19.40	19.30	25.70			$E_d/\times 10^{-4}$	3.28	4.25	4.83	4.29	6.53
			R^2	0.93	0.91	0.89	0.90	0.878			R^2	0.98	0.99	0.99	0.99	0.99
		ii	$D_a(\times 10^2)$	2.14	2.41	2.60	3.34	3.63		ii	$D_d/\times 10^2$	2.00	2.28	2.46	3.34	3.55
			$E_a(\times 10^{-4})$	8.44	11.10	17.30	15.90	22.10			$E_d/\times 10^{-4}$	4.90	4.75	4.99	5.52	7.05
			R^2	0.96	0.96	0.93	0.96	0.94			R^2	0.99	0.99	0.99	0.99	0.99
		iii	$D_a(\times 10^2)$	6.92	7.75	8.58	10.52	11.81		iii	$D_d/\times 10^2$	6.49	7.26	8.00	10.42	11.52
			$E_a(\times 10^{-4})$	8.81	11.50	17.80	16.60	23.30			$E_d/\times 10^{-4}$	4.19	4.57	4.93	5.05	6.82
			R^2	0.95	0.94	0.91	0.94	0.92			R^2	0.99	0.99	0.99	0.99	0.99

Note: i is axial strain. ii is circumferential strain. iii is volumetric strain

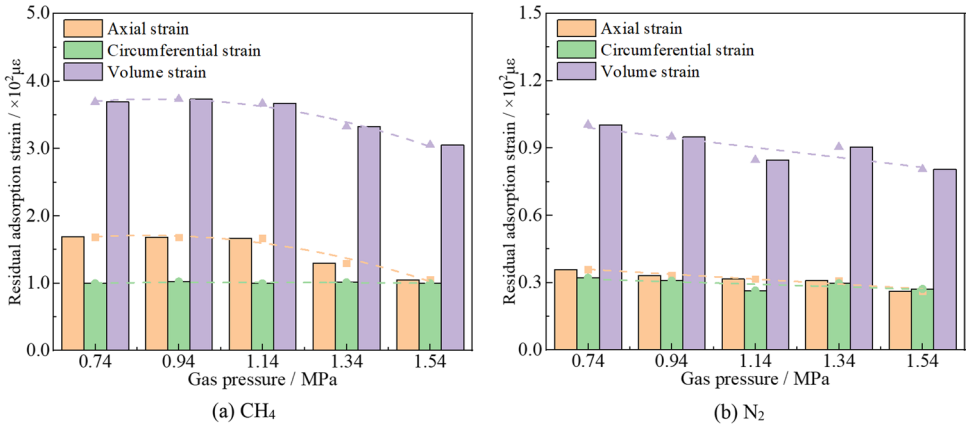

Fig. 8 Residual adsorption strain generated by coal desorption of CH_4/N_2

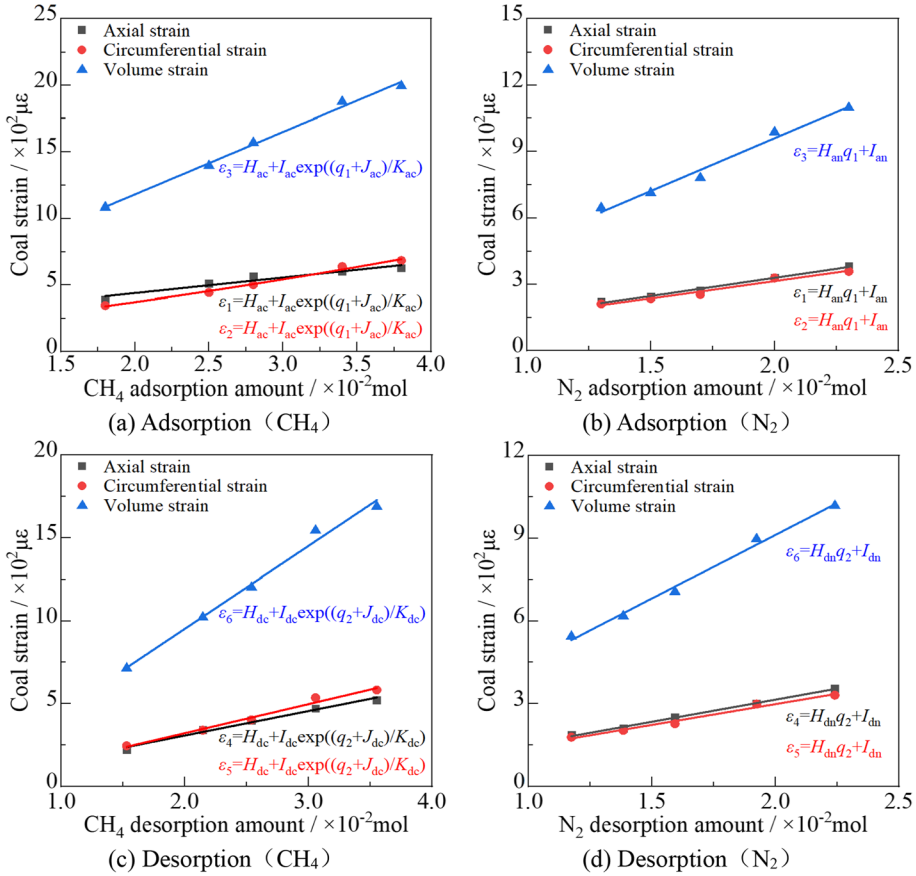

Fig. 9 Correlation between coal deformation and gas adsorption amount

monomolecular layer adsorption region and monomolecular layer free region (Zhang et al. 2022c).

Coal has a complex network of pores and fractures, and gas molecules not only have different adsorption forms in multi-level pores, but also have different migration modes. The > 1.5 nm pores consist of diffusion pores (1.5–100 nm) and seepage pores (> 100 nm). Among them, the diffusion modes of gas molecules in the diffusion pores include gas-phase diffusion, surface diffusion, and crystal diffusion, and gas-phase diffusion is dominant. The seepage modes of the gas molecules in the seepage holes include low-velocity non-Darcy flow, Darcy flow, and high-velocity non-Darcy

flow, as shown in Fig. 10. In general, most of gas molecules in coal are mainly attached to the multilevel pores in the adsorbed state, while a few gas molecules exist in the free state.

The adsorption of gas by coal belongs to physical adsorption. The strength of physical adsorption depends on the interaction between the two, which in turn affects the amount of gas adsorption. The molecular dynamics diameter, critical temperature, and diffusion velocity of the gas are important factors affecting the amount of gas adsorption. Gas with smaller molecular dynamics diameter, higher critical temperature, and faster diffusion rate is more easily adsorbed.

The basic physical parameters of CH_4/N_2 are shown in Table 7. The molecular dynamic diameter of CH_4 is larger than that of N_2, and the critical temperature and dynamic viscosity coefficient of CH_4 are smaller than those of N_2. Although N_2 can enter the coal pores with smaller sizes, the experimental coal samples have less pore-size distribution in the range of 0.36–0.38 nm, so the pore-size range accessible by CH_4/N_2 is the same. And the critical temperature and dynamic viscosity coefficient of N_2 are greater than that of CH_4, which shows that the adsorption amount of coal for CH_4 is greater than that for N_2.

5.1.2 Coal deformation characteristics

The deformation of the coal caused by gas migration is due to the combined action of adsorbed gas and free gas. The former causes expansion deformation of the coal by reducing the surface free energy of the coal matrix. The latter causes compression and deformation of the coal matrix in the form of pore pressure. Related studies show that the coal continues to expand and deform when non-adsorptive He is injected into the coal (Zhang 2015; Durucan et al. 2009). The root cause is that the gas molecules enter the pores and fractures with a spatial size greater than or equal to the average free path of the gas molecules, resulting in an increase in the volume of the pores and fractures, which is manifested as an expansion deformation of the coal at the macroscopic level.

Thus, the deformation mechanism of coal contains two main types (Lu et al. 2001): (1) Ontogenetic deformation, deformation caused by the coal matrix itself (expansion effect of adsorbed gas on coal and compression effect of free gas on coal). (2) Structural deformation, deformation resulting from relative displacement between coal matrix (expansion effect of free gas on coal). That is, the gas present in the two states produces three aspects of deformation effect on the coal, as presented in Fig. 11.

Since the ability of coal to adsorb CH_4 is greater than the ability to adsorb N_2, the reduction in surface-free energy on coal when adsorbing CH_4 is greater than the reduction in surface-free energy on coal when adsorbing N_2. Under the combined effect of the three stresses (expansion stress of adsorbed CH_4 on coal matrix, compressive stress of free CH_4 on coal matrix, expansion stress of free CH_4 on the micropores and cracks of the coal), the deformation amount of coal when adsorbing CH_4 is greater than the deformation amount of coal when absorbing N_2.

In addition, coal is a complex heterogeneous medium. The material composition, particle size, and cement make the coal have structural differences. This difference will affect the gas adsorption–desorption, which will affect the deformation of the coal itself in all directions. That is, the adsorption–desorption deformation of coal generally has anisotropic characteristics.

5.2 Anisotropy and gas-difference characteristics of coal deformation

To study the anisotropy and gas-difference characteristics of coal deformation, the anisotropy coefficients (β_1 is the ratio of the axial adsorption strain to the circumferential adsorption strain. β_2 is the ratio of the axial desorption strain to the circumferential desorption strain. β_3 is the ratio of the axial residual adsorption strain to the circumferential residual

Table 6 Fitting parameters for the adsorption–desorption strain of coal

Stage	Strain	Fitting parameters (CH_4)					Fitting parameters (N_2)		
		H_{ac}	I_{ac}	J_{ac}	K_{ac}	R^2	H_{an}	I_{an}	R^2
I	i	− 6.185E6	4.849E4	− 2.573E3	530.626	0.933	1.638E4	2.120	0.992
	ii	− 844.899	186.664	− 0.124	0.077	0.990	1.568E4	1.205	0.972
	iii	− 6.131E9	1.600E9	− 1.767E5	1.310E5	0.994	4.774E4	4.529	0.991
Stage	Strain	Fitting parameters (CH_4)					Fitting parameters (N_2)		
		H_{dc}	I_{dc}	J_{dc}	K_{dc}	R^2	H_{dn}	I_{dn}	R^2
II	i	− 1.789E9	2.585E9	4.453E4	1.210E5	0.985	1.603E4	− 5.845	0.998
	ii	− 2.203E4	1.068E3	− 3.873	1.280	0.933	1.506E4	− 2.512	0.983
	iii	− 7.104E9	2.269E8	− 4.908E5	1.425E5	0.990	4.614E4	− 10.869	0.997

adsorption strain.) are introduced to analyze the anisotropy characteristics of coal deformation, and the gas-difference coefficients (γ_1 is the ratio of the axial/circumferential strain generated by the adsorption of CH_4 to the axial/circumferential strain generated by the adsorption of N_2. γ_2 is the ratio of the axial/circumferential strain generated by the desorption of CH_4 to the axial/circumferential strain generated by the desorption of N_2. γ_3 is the ratio of the axial/circumferential strain produced by the residual CH_4 to the axial/circumferential strain produced by the residual N_2.) are introduced to analyze the gas-difference characteristics of coal deformation. Taking the experimental duration of 1.80×10^3 s as the division basis of the time nodes (T), the adsorption process was divided into eight-time nodes, and the desorption process was divided into five-time nodes.

5.2.1 Time-varying characteristics of coal deformation

The variation pattern of the anisotropy coefficient and gas discrepancy coefficient of coal deformation with experimental time is shown in Fig. 12.

Anisotropy coefficient: It can be seen from Figs. 12a, b that β_1 is relatively stable during the CH_4/N_2 adsorption process. The β_1 when coal adsorbs CH_4 and N_2 is 0.919–1.172 and 1.005–1.117, respectively. In the initial stage of CH_4/N_2 desorption, β_2 decreases slightly. The reason is that after CH_4/N_2 adsorption equilibrium, the force in the axial direction of the coal is superimposed on the gas equilibrium pressure. After the desorption experiment starts, the gas pressure at the exhaust end is instantly deflated, the axial force is decreased, and the coal first expands in the axial direction. The desorption shrinkage in the axial direction is reduced, resulting in a slight decrease in β_2. The β_2 tends to increase

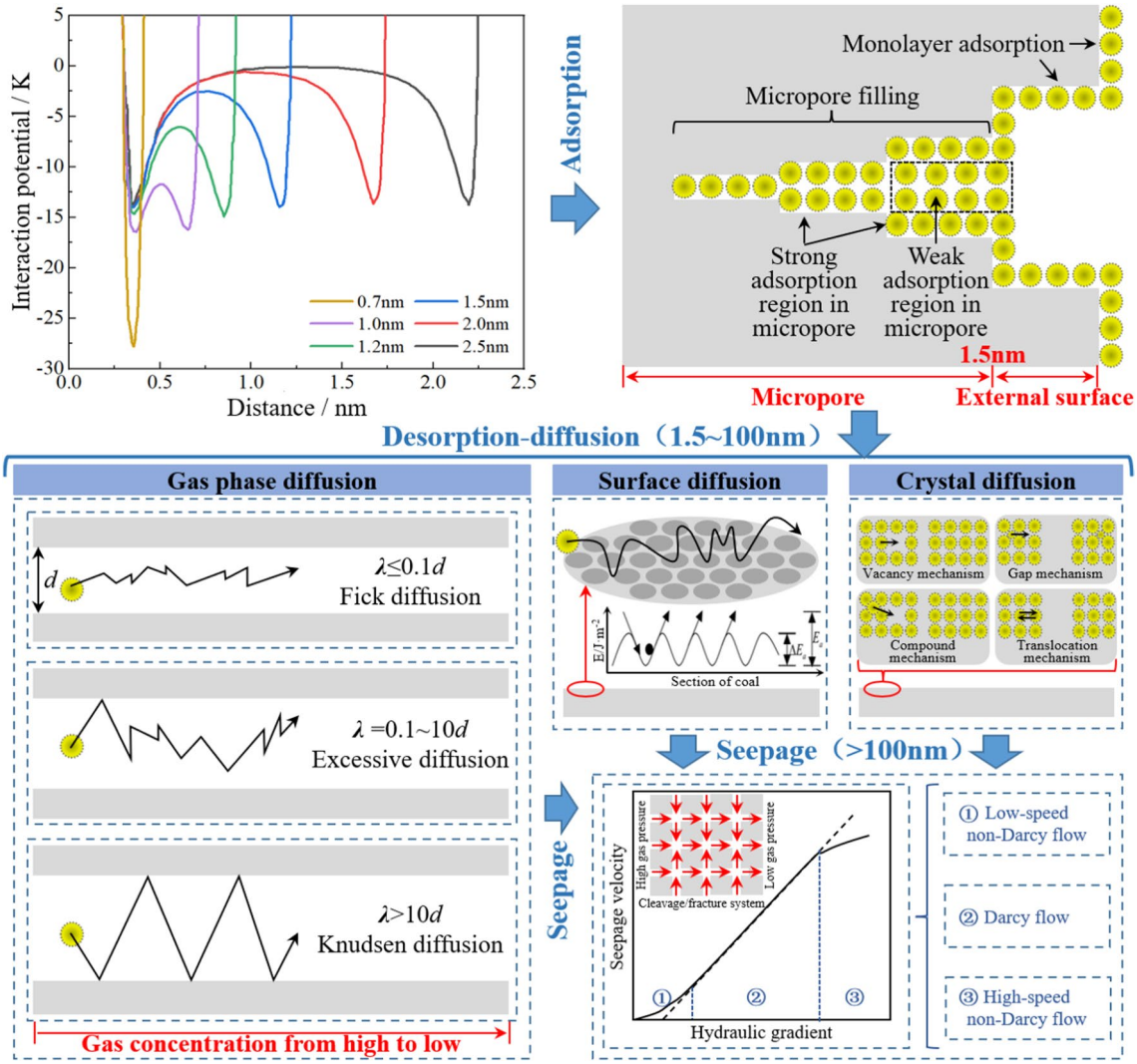

Fig. 10 Gas occurrence pattern in complex pore (modified according to reference (Zhang et al. 2022c))

Table 7 Physical parameters of CH_4/N_2

Gas type	Molecular dynamics diameter (nm)	Critical temperature (°C)	Dynamic viscosity coefficient (10^{-5} Pa s) (25 °C, 0.1013 MPa)
CH_4	0.38	− 82.6	1.03
N_2	0.36	− 147.0	1.69

as the desorption time increases. The β_2 when coal desorbs CH_4 and N_2 is in the range of 0.725–1.016 and 0.882–1.090, respectively. During the desorption of CH_4 from coal, β_3 showed an increasing trend, while there was no obvious change pattern of β_3 during the desorption of N_2.

Gas discrepancy coefficient: It can be seen from Figs. 12c, d that γ_1 is relatively stable during the CH_4/N_2 adsorption process. The γ_1 of axial strain and circumferential strain of coal are 1.621–2.215 and 1.642–1.986, respectively. In the early stage of CH_4/N_2 desorption, γ_2 decreased slightly. The reason is that after CH_4/N_2 adsorption equilibrium, the axial force on the coal superimposes the gas equilibrium pressure, and the N_2 equilibrium pressure is greater than the CH_4 equilibrium pressure. After the N_2 desorption experiment started, the axial force on the coal decreased significantly, the expansion ability in the axial direction was strong, and the desorption shrinkage decreased, while the shrinkage ability in the circumferential direction was strong, and the desorption shrinkage increased. As the desorption time prolongs, γ_2 tends to increase. The γ_2 of axial strain and circumferential strain of coal are in the range of 0.738–1.652, 0.791–1.794. During the desorption of CH_4/N_2 from coal, the γ_3 of axial strain tends to increase, while γ_3 of circumferential strain has no obvious change pattern.

5.2.2 Discrete characteristics of coal deformation

From the analysis in Sect. 5.2.1, it can be known that the adsorption strain/desorption strain of the columnar coal sample has obvious discrete characteristics. It is necessary to analyze the degree of dispersion in coal strain at each equilibrium pressure during CH_4 and N_2 adsorption/desorption, as illustrated in Fig. 13.

It can be seen from Figs. 13a–d that, (1) Adsorption process: when the CH_4 pressure is ≤ 1.14 MPa, the axial adsorption strain is larger than the circumferential adsorption strain. When the CH_4 pressure is ≥ 1.34 MPa, the axial adsorption strain is smaller than the circumferential adsorption strain. The axial adsorption strain was greater than the circumferential adsorption strain in the experimental N_2 pressure range. It is because the bedding structure of the coal sample is perpendicular to the axial direction of the coal, and the adsorption deformation amount in the vertical bedding direction is stronger, which shows that the axial adsorption strain is larger than the circumferential adsorption strain

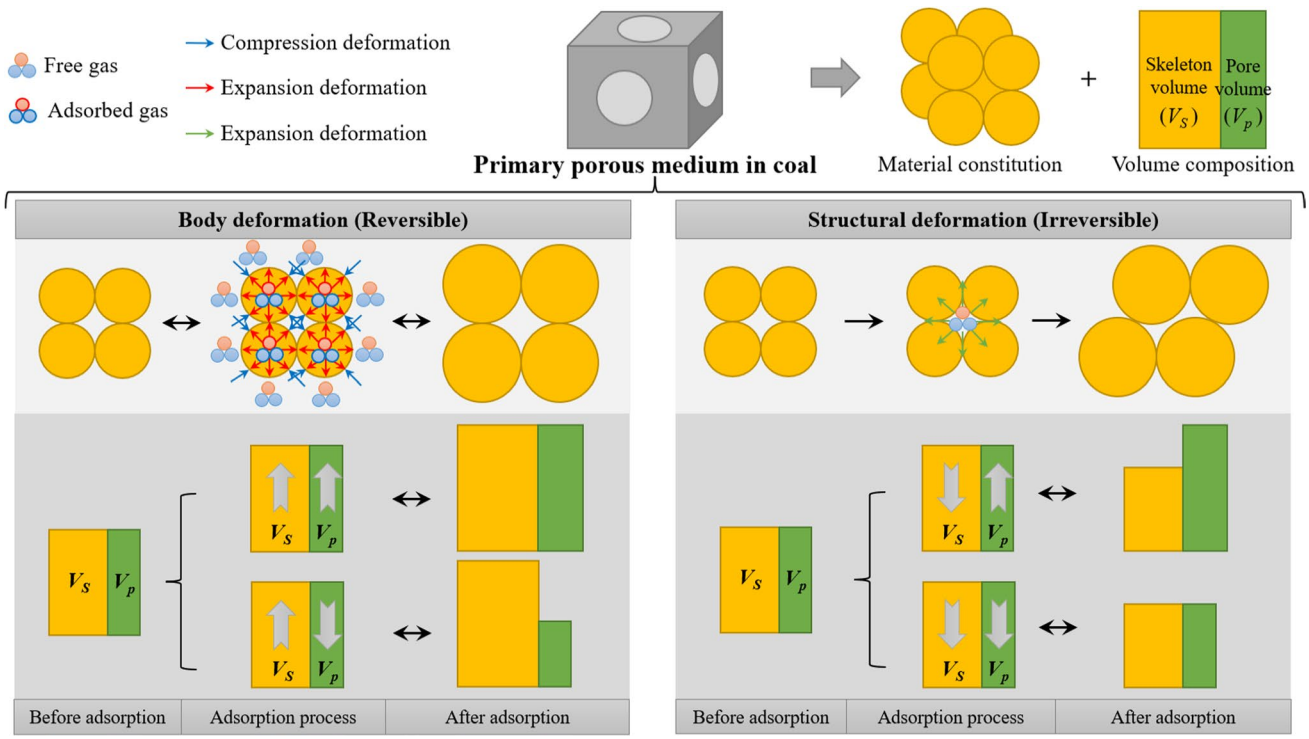

Fig. 11 Coal deformation characteristics in complex pore

when the CH_4/N_2 pressure ≤ 1.14 MPa. With the increase of CH_4 pressure, the amount of gas adsorbed by coal increases, the reduction of surface-free energy increases, and the strength decreases significantly. Moreover, a larger expansion strain is generated in the circumferential direction where the force is smaller, indicating that the axial adsorption strain is smaller than the circumferential adsorption strain when the CH_4/N_2 pressure ≥ 1.34 MPa. (2) Desorption process: The total axial desorption strain is generally smaller than the circumferential desorption strain in the CH_4 pressure range, and the axial residual strain is larger than the circumferential residual strain. When the CH_4 pressure is ≤ 1.14 MPa, the change of β_3 is not obvious. When the CH_4 pressure ≥ 1.34 MPa, β_3 shows a gradually decreasing trend. The dispersion of β_2 and β_3 is large during the desorption of N_2 from coal.

It can be seen from Figs. 13e–h that $\gamma_1 > 1$ for CH_4/N_2 adsorption and γ_2 total > 1 and $\gamma_3 > 1$ for CH_4/N_2 desorption by coal. It indicates that the axial strain and circumferential strain generated by the adsorption/desorption of CH_4 in coal are greater than those generated by the adsorption/desorption of N_2. γ_3 for residual CH_4/N_2 in coal > γ_1 for adsorption of $CH_4/N_2 > \gamma_2$ for desorption of CH_4/N_2 at the same time nodes.

In summary, the dispersion of β_1 and γ_1 at each time node during the CH_4/N_2 adsorption process is large for gas pressures ranging from 0.74 to 1.14 MPa. As the gas pressure increases, the dispersion of β_1 and γ_1 at each time node decreases. During the CH_4/N_2 desorption process, with the increase of CH_4 pressure, the dispersion of γ_2 remains unchanged while the discreteness of β_3 decreases. With the increasing pressure of N_2, the dispersion of β_3 and γ_3 has no obvious change rule.

5.3 Strain model of coal adsorption–desorption CH_4/N_2

Coal adsorption/desorption deformation involves coal–gas interaction and the mechanical behavior of gas adsorption/desorption (Chen et al. 2018; Zhao et al. 2013). From the analysis in Sect. 5.1.2, it can be known that the stress in the process of gas adsorption/desorption includes three types. The adsorption/desorption deformation of coal is the result of the coupling effect of three kinds of stress (the gas adsorption deteriorates the mechanical characteristics of coal, resulting in obvious compression deformation of coal. The effect of pore pressure changes its own pore and fracture structure, which in turn affects the amount of gas adsorption and coal deformation.) (Liu et al. 2018; Sun et al. 2023). Simply analyzing the coal deformation caused by three types of stresses separately not only ignores the complex coupling relationship among the three, but also leads to the establishment of a more complicated coal strain model. Therefore, it can be considered to study the comprehensive

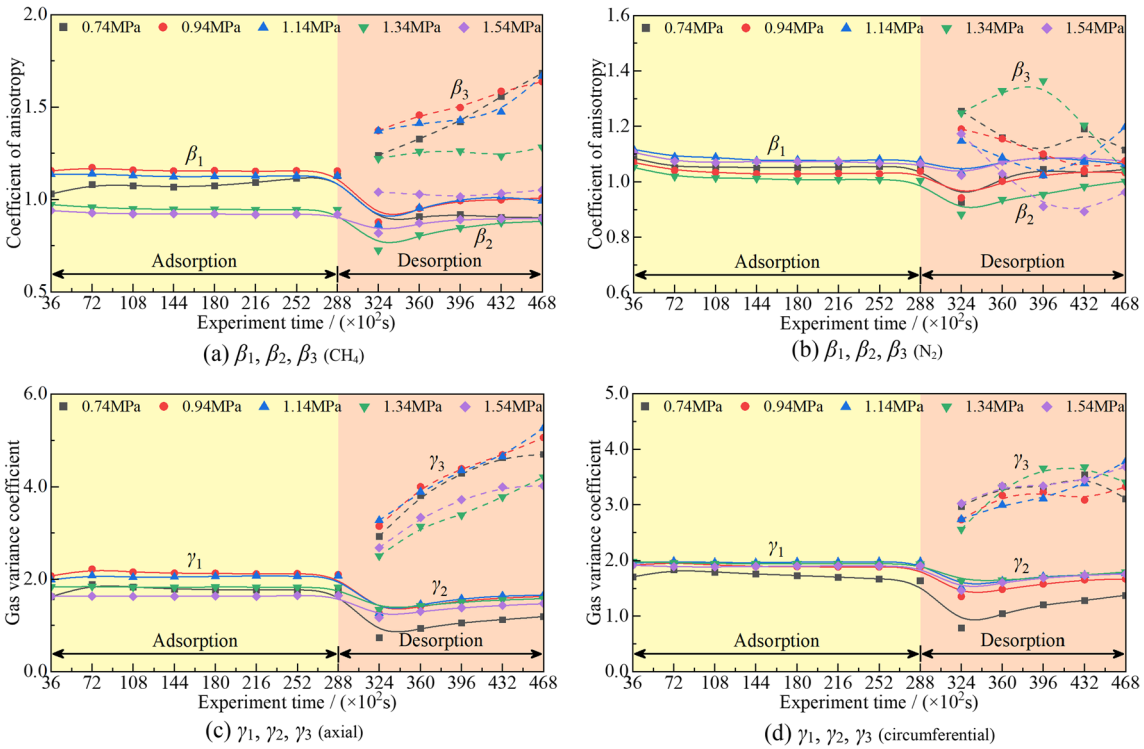

Fig. 12 Time-varying characteristics of coal deformation

effects of three stresses on coal deformation from an overall perspective.

From the analysis in Sects. 4.1 and 4.2, it can be known that the variation law of CH_4/N_2 adsorption amount with adsorption time and desorption time, as well as the variation law of strain generated by CH_4/N_2 adsorption on coal with adsorption time and desorption time are consistent with the Langmuir-type equation. To eliminate the effect of time effect, Eq. 1 is substituted into Eq. 2. Establish the relationship model between gas adsorption amount and coal adsorption strain in the whole process of CH_4/N_2 adsorption experiment, and the relationship model between gas adsorption amount and coal desorption strain in the whole process of CH_4/N_2 desorption experiment, as shown in Eq. (3).

$$\begin{cases} \varepsilon_a = D_a E_a Q_a / (A_a B_a + E_a Q_a - B_a Q_a) + F_a \\ \varepsilon_d = (D_d E_d Q_d - D_d E_d C_d) / (A_d B_d - B_d C_d + B_d Q_d - E_d Q_d + E_d C_d) + F_d + G_d \end{cases} \tag{3}$$

Taking the axial/circumferential adsorption strain and axial/circumferential desorption strain of coal under different CH_4/N_2 pressures as examples, the applicability and reliability of the coal strain model (Eq. (3)) were verified. The fitting results of the coal strain model are shown in Fig. 14.

The proposed model has a large error in fitting coal adsorption strain data and a small error in fitting coal desorption strain data. This is because the columnar raw coal has a certain spatial scale, and under the same adsorption time, the deformation degree at each position of the raw coal is different. Since the sticking position of the strain gauge is attached to the middle of the coal sample, the adsorption

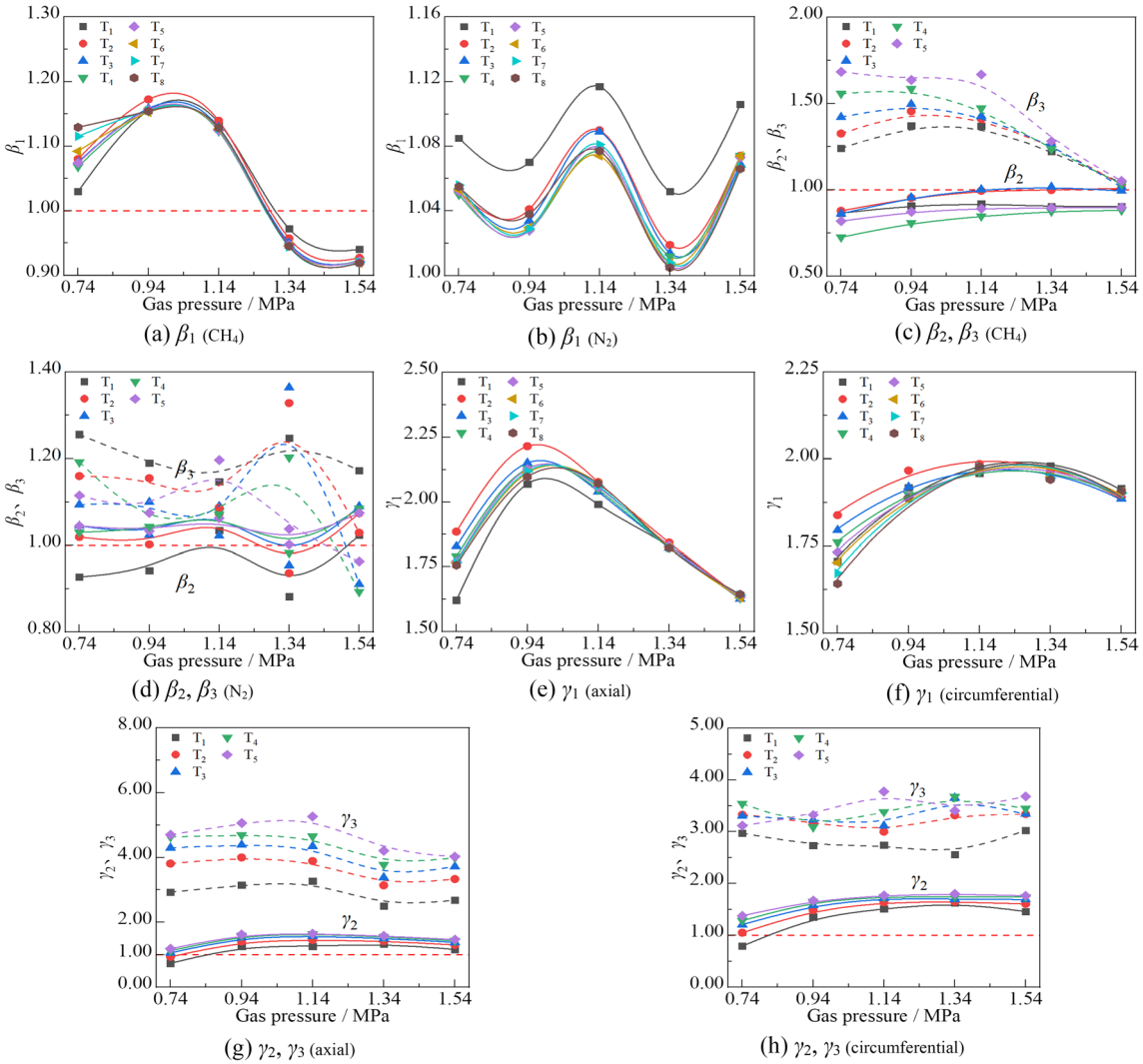

Fig. 13 Discrete characteristics of coal deformation

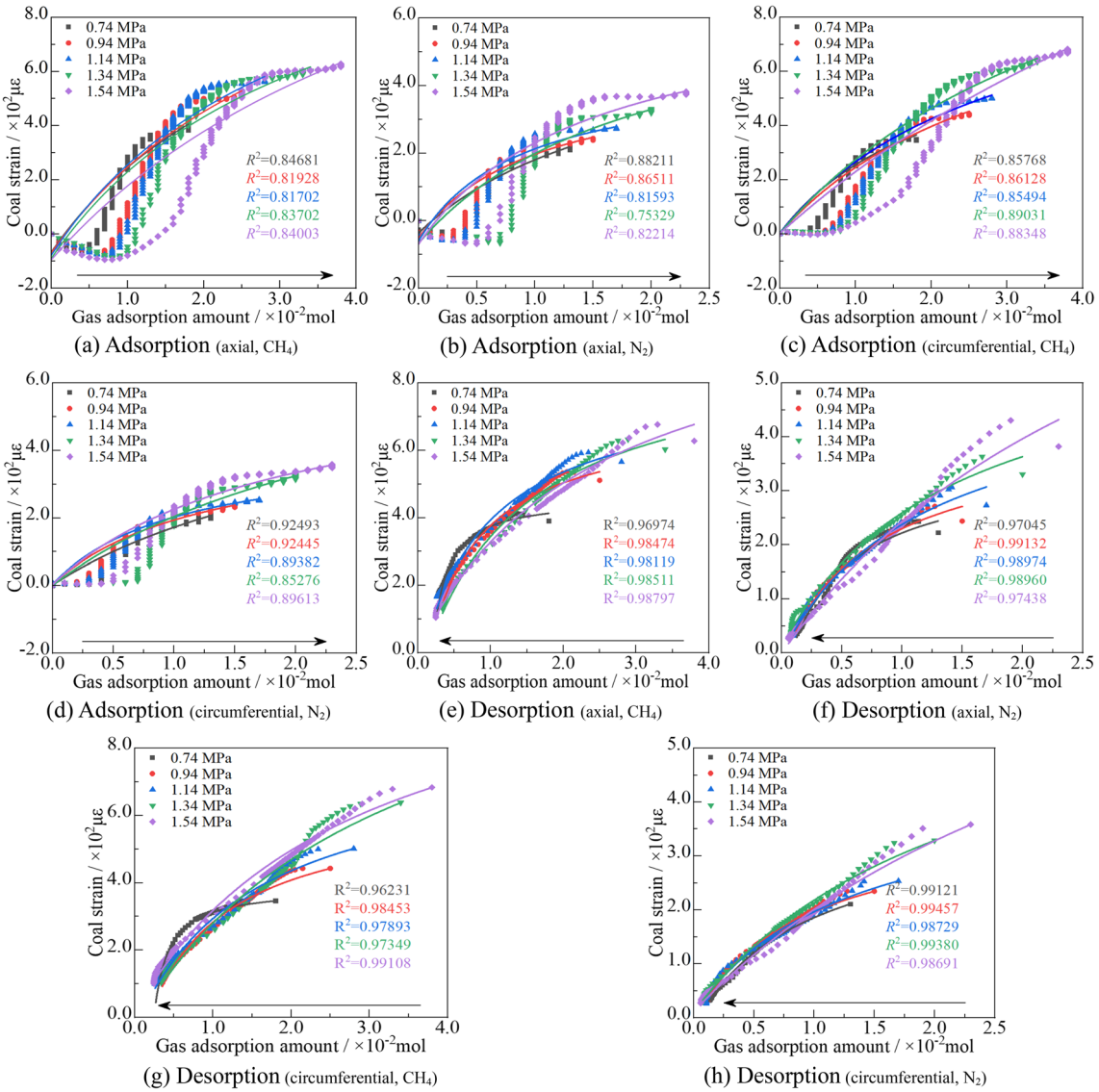

Fig. 14 Strain model of coal adsorption–desorption CH_4/N_2

strain lags behind the gas adsorption amount, and the desorption strain leads the gas adsorption amount. Generally, the coal strain model has a high degree of fit, which can reflect the correlation between gas adsorption amount and coal strain amount in each stage of CH_4/N_2 adsorption–desorption to some extent.

5.4 Applicability of N_2 injection displacement CH_4 technology to low-permeability coal

The applicability of the N_2 injection for CH_4 displacement technology to the gas occurrence characteristics in low-permeability coal seams requires comprehensive consideration of the following three aspects:

(1) Displacement effect: Under the same gas pressure, the equilibrium time of coal adsorption/desorption of N_2 is shorter than that of adsorption/desorption of CH_4 (for example, when the gas pressure is 1.14 MPa, the time to reach the equilibrium of CH_4/N_2 adsorption by coal is 2.600×10^4 s, 1.558×10^4 s). And the dynamic viscosity coefficient of N_2 is smaller than that of CH_4, which makes N_2 have a very good carrying effect of CH_4, thus realizing the increase of CH_4 flow in coal seam (Yang et al. 2016; Ji et al. 2023).

(2) Economic benefits: As an important component of air, N_2 comes from a variety of sources. There are various ways to produce N_2, the process of N_2 production is mature, and the cost of N_2 production is low. After N_2 is mixed into CH_4, it is not easy to make it lose its

combustion and utilization value, which is beneficial to the utilization of CH_4 resources (Hao et al. 2016). In addition, a reasonable and effective field construction process of N_2 injection for CH_4 replacement should be adopted to increase the CH_4 volume fraction of the mixed gas and reduce the separation and purification costs in the process of the CH_4 utilization process, thereby improving the economic efficiency.

(3) Safety issue: Under the same gas pressure, the strain of coal absorbs/desorbs N_2 is smaller than that of absorbs/desorbs CH_4 (for example: when the gas pressure is 1.14 MPa, the equilibrium strains when coal adsorbs CH_4/N_2 are 565.95με and 273.21με.), which makes the outburst danger of N_2 injected into the coal seam weaker than that of CH_4, and the safety risk of N_2 leakage is small (Lin et al. 2023c).

In summary, N_2 has good injectability in low-permeability coal seams and has the dual function of improving coal seam permeability and enhancing gas flow. N_2 injection for CH_4 displacement technology can not only improve the effect of gas management in low-permeability coal seams but also effectively reduce the cost of gas injection and increase the profit per ton of coal, thus effectively promoting the efficient utilization of coal seam gas resources.

6 Conclusions

(1) Micropores and transition pores are relatively developed in coal samples, and the pore morphology is mainly semi-open pores. The pore structure is highly complex and heterogeneous. The tortuosity of the coal sample is 5.81, the effective porosity is 3.04%, and the pore connectivity is 40.36%. As the pore-size increases, the proportion of pores in each pore-size segment decreases, and the pore connectivity ratio increases, indicating that the connectivity of the seepage pores is good, and the connectivity of the adsorption pores is poor.

(2) Under the condition of constant triaxial stress, the ability of coal to adsorb CH_4 and its ability to adsorb CH_4 deformation is greater than that of N_2. The evolution law of strain (axial strain, circumferential strain, volumetric strain) with experimental time for the whole process of CH_4/N_2 adsorption–desorption by coal can be divided into three stages. The variation pattern of coal strain produced by CH_4/N_2 adsorption–desorption with the experimental time conforms to the Langmuir-type equation.

(3) The change law of coal strain produced by CH_4/N_2 adsorption–desorption with the experimental time corresponds to the Langmuir-type equation. The expansion strain of the coal increases exponentially as a function of CH_4 adsorption. The desorption shrinkage strain of coal increases exponentially as a function of CH_4 desorption.

(4) The deformation caused by the adsorption–desorption of CH_4/N_2 in coal has anisotropic and gas-difference. A strain model for the adsorption–desorption of CH_4/N_2 from coal was established by considering the expansion stress of adsorbed gas on the coal matrix, the compression stress of free gas on the coal matrix, and the expansion stress of free gas on micropore fractures, which effectively reflects the correlation between the process gas adsorption and coal strain amount at each stage of CH_4/N_2 adsorption–desorption experiment.

(5) N_2 has good injectability in low-permeability coal seams and has the dual functions of improving coal seam permeability and enhancing gas flow, which not only effectively improves the effect of gas management in low-permeability coal seams, but also reduces the cost of gas injection, increases the profit per ton of coal, and promotes the efficient utilization of gas resources.

Acknowledgements This study was financially supported by the Natural Science Foundation of China (51874236 and 52174207), Shaanxi Provincial Department of Science and Technology (2020JC-48 and 2022TD-02), and China Postdoctoral Science Foundation (2021M693879).

Declarations

Competing interests The authors declare that they have no known competing financial interests or personal relationships that could appear to have influenced the work reported in this paper.

References

Attia AM (2005) Effects of petrophysical rock properties on tortuosityfactor. J Petrol Sci Eng 48(3–4):185–198

Chen J, Pan XK, Jiang DY et al (2018) Adsorption deformation characteristics of soft coal and hard coal to different gases under triaxial stress condition. J China Coal Soc 43(S1):149–157

Chen XJ, Zhao S, Si ZX et al (2020) Fractal characteristics of pore structure of coal with different metamorphic degrees and its effect on gas adsorption characteristics. Coal Sci Technol 48(2):118–124

Cheng YP, Hu B (2021) Main occurrence form of methane in coal: micropore filling. J China Coal Soc 46(9):2933–2948
Cheng YP, Hu B (2023) A new pore classification method based on the methane occurrence and migration characteristics in coal. J China Coal Soc 48(1):212–225
Dullien FAL (2012) Porous media: fluid transport and pore structure. Academic Press, New York
Durucan S, Ahsan M, Shi JQ (2009) Matrix shrinkage and swelling characteristics of European coals. Energy Procedia 1(1):3055–3062
Gregg SJ, Sing KSW (1982) Adsorption surface are and porosity. St Edmundsbury Press, London
Hao DY, Ye ZW, Fang SL (2016) Prospect situation and prospect of coal seam gas recovery by gas injection technology utilization in China. China Min Mag 25(7):77–81
He W, Liang WG, Zhang BN et al (2018) Experimental study on swelling characteristics of CO_2 adsorption and storage in different coal rank. J China Coal Soc 43(5):1408–1415
Hodot BB (1966) Coal and gas outburst. China Industry Press, Beijing (**Song Shizhao, translated**)
Hu B, Cheng YP, Pan ZJ (2023) Classification methods of pore structures in coal: a review and new insight. Gas Sci Eng 110:204876
Ji PF, Lin HF, Kong XG et al (2023) Experimental study on enhanced coal seam gas extraction by uniform pressure/pulse pressure N_2 injection. Fuel 351:128988
Jia TF, Wang M, Gao XY et al (2021) Pore structure characteristics of low-rank coal reservoirs and evaluation of fractal models. Nat Gas Geosci 32(3):423–436
Jiang JY, Cheng YP, Zhang S (2021) Quantitative characterization of pore structure and gas adsorption and diffusion properties of low-rank coal. J China Coal Soc 46(10):3221–3233
Jin YR, Huang ZX (2015) Adsorption and pore size distribution. National Defence Industry Press, Beijing
Li XC, Zhang L, Zhao JF et al (2018) Coal deformation characteristics in gas adsorption and desorption. J Min Sci Technol 3(1):46–54
Li SG, Zhou YX, Hu B et al (2023) Adsorption pore structure characteristics of low rank coal and effect on methane adsorption performance. Coalf Geol Explor 51(4):127–136
Lin J, Ren T, Wang GD et al (2017) Experimental study of the adsorption-induced coal matrix swelling and its impact on ECBM. J Earth Sci 28(5):917–925
Lin HF, Bu JT, Yan M et al (2019) Joint analysis of pore structure characteristics of middle and low rank coal with nitrogen adsorption and mercury intrusion method. J xi'an Univ Sci Technol 39(1):1–8
Lin HF, Ji PF, Kong XG et al (2023a) Temporal and spatial characteristics of raw coal deformation during the adsorption of CH_4/N_2 under triaxial stress. J China Univ Min Technol 52(2):314–328
Lin HF, Ji PF, Kong XG et al (2023b) Experimental study on the influence of gas pressure on CH_4 adsorption–desorption–seepage and deformation characteristics of coal in the whole process under triaxial stressmain. Fuel 333:126513
Lin HF, Ji PF, Kong XG et al (2023c) Progress and prospect of gas extraction technology by underground gas injection displacement for increasing flow in low-permeability coal seam in China. J China Coal Soc 48(2):730–749
Liu LY, Zhu WC, Wei CH et al (2018) Mechanical model and numerical analysis of mechanical property alterations of coal induced by gas adsorption. Rock Soil Mech 39(4):1500–1508
Liu YW, Zhang S, Zuo WQ et al (2021) Study on the difference of pore structure of typical soft and hard coal. Coal Sci Technol 49(10):98–106
Liu HQ, Wang L, Xie GX et al (2022) Comprehensive characterization and full pore size of fractal characteristics of coal pore structure. J Min Saf Eng 39(3):458–469
Lu SQ (2016) Mechanism failure and permeability evolution mechanism of coal based on equivalent matrix scale and its application. China University of Mining and Technology, Xuzhou
Lu P, Shen ZW, Zhu GW et al (2001) The effective stress and mechanical deformation and damage characteristics of gas-filled coal. J China Univ Sci Technol 31(6):687–693
Meng Y, Li ZP, Tang SH et al (2021) Laboratory investigation on methane sorption-induced strain and permeability in middle and high rank coal samples. J China Coal Soc 46(6):1915–1924
Ortiz L, Kuchta B, Firlej L et al (2016) Methane adsorption in nanoporous carbon: the numerical estimation of optimal storage conditions. Mater Res Express 3(5):55011
Ranjith PG, Jasinge D, Choi SK et al (2010) The effect of CO_2 saturation on mechanical properties of Australian black coal using acoustic emission. Fuel 89(8):2110–2117
Sang SX, Zhu YM, Zhang SY et al (2005) Solid–gas interaction mechanism of coal-adsorbed gas (I)—coal pore structure and solid–gas interaction. Nat Gas Ind 25(1):13–15
Sun FR, Liu DM, Cai YD et al (2023) Coal rank-pressure coupling control mechanism on gas adsorption/desorption in coalbed methane reservoirs. Energy 270:126849
Wang ZY, Cheng YP, Wang G et al (2022) Comparative analysis of pore structure parameters of coal by using low pressure argon and nitrogen adsorption. Fuel 309:122120
Wen YZ, Ni GH, Zhang XY et al (2023) Fine characterization of pore structure of acidified anthracite based on liquid intrusion method and Micro-CT. Energy 263:125639
Xie MH, Huang YY (1985) Surface physical chemistry. China Building Industry Press, Beijing
Yang HM, Feng ZY, Chen LW (2016) Analysis of replacement-displacement effect and its change mechanism in simulation experiment of nitrogen injection into coal seam. J China Coal Soc 41(9):2246–2250
Yu BM, Li JH, Li ZH et al (2003) Permeabilities of unsaturated fractal porous media. Int J Multiph Flow 29(10):1625–1642
Zhang ZG (2015) Study on characteristics of adsorption/desorption-induced deformation and its influencing factors. Chongqing University, Chongqing
Zhang XD, Zhang S, Du ZG et al (2021) CO_2 and N_2 adsorption/desorption effects and thermodynamic characteristics in confined coal. J Petrol Sci Eng 207:109166
Zhang KZ, Zou AA, Wang L et al (2022a) Multiscale morphological and topological characterization of coal microstructure: insights into the intrinsic structural difference between original and tectonic coals. Fuel 321:124076
Zhang ZG, Chen Y, Tang C et al (2022b) Deformation characteristics and model of coal adsorption/desorption on CO_2. J China Coal Soc 47(8):3128–3137
Zhang KZ, Cheng YP, Wang L et al (2022c) Pore network structure characterization based on gas occurrence and migration in coal. J China Coal Soc 47(10):3680–3694
Zhao HB, Li HH, Du QH et al (2013) Experimental study of coupling relationship between lateral strain of coal containing gas and characteristics of gas flow. Rock Soil Mech 34(12):3384–3388
Zhu J, He F, Xu LH et al (2018) Relationship of coal pore structure and adsorption/desorption strain. Coal Technol 37(6):145–147